Applied Catalysis B: Environmental 234 (2018) 100–108

Contents lists available at ScienceDirect

Applied Catalysis B: Environmental

journal homepage: www.elsevier.com/locate/apcatb

Surface states as electron transfer pathway enhanced charge separation in TiO_2 nanotube water splitting photoanodes

Heng Zhu[a], Meiming Zhao[a], Junkang Zhou[b], Wenchao Li[a], Haoyu Wang[b], Zhe Xu[a], Lei Lu[a], Lang Pei[a], Zhan Shi[b], Shicheng Yan[a,*], Zhaosheng Li[a], Zhigang Zou[a,b,c]

[a] Eco-Materials and Renewable Energy Research Center (ERERC), Collaborative Innovation Center of Advanced Microstructures, College of Engineering and Applied Sciences, Nanjing University, No. 22, Hankou Road, Nanjing, Jiangsu, 210093, PR China
[b] Jiangsu Key Laboratory for Nano Technology, National Laboratory of Solid State Microstructures, Department of Physics, Nanjing University, No. 22, Hankou Road, Nanjing, Jiangsu, 210093, PR China
[c] Macau Institute of Systems Engineering Macau University of Science and Technology, Macau 999078, PR China

ARTICLE INFO

Keywords:
Photoelectrocatalysis
TiO_2 nanotube
Mott-Schottky (M-S)
Surface states
Charge separation

ABSTRACT

Surface states on TiO_2 photoanodes are usually considered to hinder the photoelectrochemical (PEC) water splitting *via* slowing charge transport and increasing charge recombination. Here, we found that electrochemically doping the TiO_2 nanotubes electrode at a potential negative than its flat band potential will induce the insertion of protons into the lattice of TiO_2 *via* a reaction of $Ti^{IV}O_2 + e^- + H^+ = Ti^{III}O(OH)$ to form the surface states. Photoelectrochemical/electrochemical tests confirmed that the surface states (Ti-OH) are an important photogenerated electron transfer route, significantly increasing charge separation efficiency, and hence contributing to the PEC performance enhancement. In addition, we have made a self-consistent explanation on Mott-Schottky (M–S) plots of the TiO_2 nanotubes electrode, demonstrating that the M–S measurement is able to accurately describe electron filling and extraction into/from surface states and not suitable to determine the flat band potential of nanostructured TiO_2 electrodes. Our results offer a new insight to understanding the role of surface states during the charge separation, transfer, and injection processes of the water splitting reaction.

1. Introduction

Photoelectrochemical (PEC) water splitting by semiconductor photoelectrodes is a potential approach to convert intermittent sunlight into fuels and chemicals. To apply this technique to a large-scale practice, a key challenge is to accelerate oxygen-evolving reaction (OER), a rate-determining step for overall water splitting due to the four-electron process requiring high overpotentials [1]. Developing efficient n-type semiconductor photoanode is the main route to challenge the OER kinetic limit. After contacted with electrolyte, a band bending formed at the semiconductor-electrolyte interface, called the semiconductor liquid junction (SCLJ) [2]. Under illumination, SCLJ is responsible for the separation and transfer of photogenerated charges and is sensitive to the microstructure of semiconductor. Enlarging the volume ratio of SCLJ by constructing nanoarchitectures is considered an effective route to improve the PEC performance of semiconductor photoelectrodes. However, nanosizing will lead to the increment of crystal defects, inducing the formation of surface electron states that fall within the band gap of the semiconductor [3–8]. Surface sates can exert great influence on both the thermodynamics and kinetics of PEC water oxidation processes [2,9–16]. Surface states may cause Fermi level pinning in some semiconductor photoanodes [2,13], which induces the increase of the overpotentials of PEC water oxidation [9,11,13]. Surface states may act as charge recombination centers [10,16] or active sites for hole accumulation and hole transfer reactions [11]. Surface states can also trap photogenerated electrons and transfer them to the electrolyte [14] or accumulate them at the photoelectrode/electrolyte interface to form an electrostatic field, leading to photoactivity decay [15].

Recently, a standpoint was supposed that the trap states on TiO_2 could be filled and passivated permanently if a highly negative bias is applied to enable protons or Li to insert into the semiconductor lattice. Such “trap-filling” effect can improve the supercapacitive and PEC performance of TiO_2 electrodes [17–28]. Unfortunately, trap states passivation effect cannot be used to explain the improved capacitance of TiO_2 electrodes, in which the charge carrier density was greatly increased after electrochemical doping of protons or other cations [17–19]. Clarifying the inconsistency in understanding the

* Corresponding author.
E-mail address: yscfei@nju.edu.cn (S. Yan).

https://doi.org/10.1016/j.apcatb.2018.04.040
Received 21 February 2018; Received in revised form 4 April 2018; Accepted 17 April 2018
Available online 19 April 2018
0926-3373/

electrochemical and photoelectrochemical results is beneficial to discover the real effects of surface states on the photo/electrochemical processes.

Here, we use TiO_2 nanotubes with high surface area as photoanode to discover the nature of surface states and their effects on charge transfer processes. We found that the surface states, Ti-OH groups, on the TiO_2 nanotubes photoanode are not the recombination centers but facilitate the separation of electron-hole pairs. The photogenerated electrons trapped in the surface states have a long-lived time and can be extracted to the conductive substrate at the applied potentials. The photo/electrochemical tests indicated that electrochemical doping H into the lattice of TiO_2 significantly enlarges the capacitance of surface states due to the increased Ti-OH surface state density, thus enhancing the photocurrent of the TiO_2 nanotubes photoanode. Finally, we have proposed a self-consistent understanding of the experimental results from the Mott-Schottky and spectro/photoelectrochemical tests.

2. Experiment methods

2.1. Preparation of TiO_2 nanotube array electrodes

The electrochemical anodic oxidation method was used to fabricate the TiO_2 nanotube arrays film [29]. To remove the surface oxidation layer, the titanium sheet (0.2 mm thickness, 99.5% purity) was first chemically polished in the solution containing HF, HNO_3, and deionized water (1:2:7 in volume) for 30 s. The resulting titanium sheets were ultrasonically cleaned with acetone, ethanol, and deionized water, and then were anodized in 250 mL NH_4F-containing ethylene glycol (EG) solution (1 g NH_4F, 245 mL EG, 5 m L deionized water) at 60 V for 15 min at room temperature and the counter electrode was a platinum plate. The as-anodized samples were thoroughly cleaned with deionized water and then annealed in air at 450 °C for 2 h with a heating rate of 10 °C min^{-1}.

2.2. TiO_2 nanotube array characterizations

The morphologies of the TiO_2 nanotube photoanodes were observed by field-emission scanning electron microscope (FE-SEM; Nova NanoSEM 230, FEI) and the transmission electron microscope (TEM; JEM-200CX, JOLE). Crystal phases of these samples were determined using an X-ray diffractometer (XRD, Rigaku Ultima III, Japan) operated at 40 kV and 40 mA using Cu Ka radiation. X-ray photoelectron spectroscopy (XPS) measurements were carried out on a Thermo VG Scientific ESCALAB 250 spectrometer with monochromatized Al Kα excitation. The spectral positions were corrected by normalizing the C 1 s spectrum at 284.6 eV, and a Shirley background was used for peak fitting. The diffuse reflection using Fourier transform spectroscopy (DRIFTS) was obtained to characterize the surface properties of the samples with a silver mirror background (NEXUS870, Nicolet, USA). Typically, 40 scans were accumulated in each spectrum. The UV–vis absorption spectra were obtained by ultraviolet-visible spectrophotometer (UV, Shimadzu UV-2550).

2.3. Electrochemical and photoelectrochemical characterization

A CHI760E electrochemical workstation (Shanghai Chenhua Company, Shanghai, China) was used to conduct the electrochemical and photoelectrochemical measurements, which were performed in a standard three-electrode cell at room temperature. The electrode except the semiconductor-electrolyte interface was thoroughly sealed with silica gel or black insulating tape. A platinum plate and saturated Ag/AgCl were used as counter and reference electrodes, respectively. All the potentials are described by referring to the Ag/AgCl reference electrode. A 500 W Xe lamp was used as the light source for photocurrent measurements. The irradiated area was circular with area of 0.28 cm^2 and photocurrent densities were normalized to 1 cm^2. Open circuit potential (OCP) decay was measured by holding the samples under illumination for 200 s at OCP or holding the samples under certain potential at *i–t* mode and then quickly switch to OCP mode monitoring the voltage decay as a function of time. Mott-Schottky curves were measured using an electrochemical analyzer (2273, Princeton Applied Research, AMETEK, USA).

2.4. Electrochemical doping

The TiO_2 nanotubes electrode as the working electrode were immersed in 1 M NaOH solution. Then a negative bias -1.35 V was applied in the dark at room temperature for 10 ~ 60 s. In addition, the TiO_2 nanotubes electrode was overdoped at a more negative bias -1.5 ~ -1.8 V.

2.5. Detection of electron transfer process

The optical spectroscopies were used to detect the trapped electrons at the surface of the TiO_2 nanotubes photoanode. Spectroelectrochemical measurements were carried out with a homemade three-electrode cell inserted in the sample compartment of the spectrophotometer at room temperature. Diffuse reflectance spectroscopy was used to monitor the absorption changes of the TiO_2 nanotube array electrode at different applied potentials. The cyclic voltabsorptograms were monitored at 720 nm and the cyclic voltammetry (CV) curves were recorded simultaneously. Cationic dye methylene blue (MB) solution (10 mg L^{-1}) was used as a probe molecule to show the electron accumulation on the surface of TiO_2 nanotubes. A -0.8 V bias was applied to TiO_2 nanotube electrode for 4 h to ensure the MB adsorption equilibrium. Then the electrodes were immersed in 10 mL deionized water for 24 h to dissolve the MB adsorbed on the TiO_2 nanotube array surface into aqueous solution. The MB concentration were measured by the UV–vis spectrophotometer. The electron accumulation on the surface of TiO_2 nanotubes was also probed by phenolphthalein reagent. The fresh-prepared phenolphthalein (0.5 wt.%) -containing ethanol solution (0.25 mL) was added into 0.5 M Na_2SO_4 electrolyte, and the color change of the TiO_2 electrode was recorded by camera at applied square wave potential oscillation between 0.8 V and -0.9 V.

2.6. Theoretical calculations

The calculations were carried out using density functional theory plus Hubbard U (DFT + U) with the Perdew-Burke-Ernzerbof (PBE) form of generalized gradient approximation functional (GGA) [30,31]. The Vienna ab-initio simulation package (VASP) [32,33] was employed. The plane wave energy cutoff was set as 400 eV. The Fermi scheme was employed for electron occupancy with an energy smearing of 0.1 eV. The first Brillouin zone was sampled in the Monkhorst − Pack grid [34]. The 4 × 4 × 1 k-point mesh for the calculations. The energy (converged to 1.0×10^{-6} eV/atom) and force (converged to 0.01 eV/Å) were set as the convergence criterion for geometry optimization. The spin polarization was considered in all calculations. The (101) surface is obtained by cutting the TiO_2 along [101] direction with the O termination. In all structural optimization calculations, the atoms with the bulk property are fixed, while the positions of the other atoms were allowed to relax. A vacuum layer as large as 12 Å was used along the c direction normal to the surface to avoid periodic interactions.

Charge redistribution was carried out on the anatase TiO_2 (101) surface with adsorption of hydrogen on bridge oxygen (O_b). The charge redistribution is calculated by equation $\Delta\rho = \rho - (\rho_s + \rho_a)$, where ρ is the charge density integrated over the unit cell of the hydrogen covered anatase TiO_2 (101) surface; ρ_s is the charge density of the bare anatase TiO_2 (101) surface, which is generated by freezing the substrate Ti and O atom positions prior to removing the adsorbates; ρ_a is the charge density of the frozen hydrogen overlayer generated by removing the TiO_2 slab. Furthermore, Bader charge analysis was applied to this

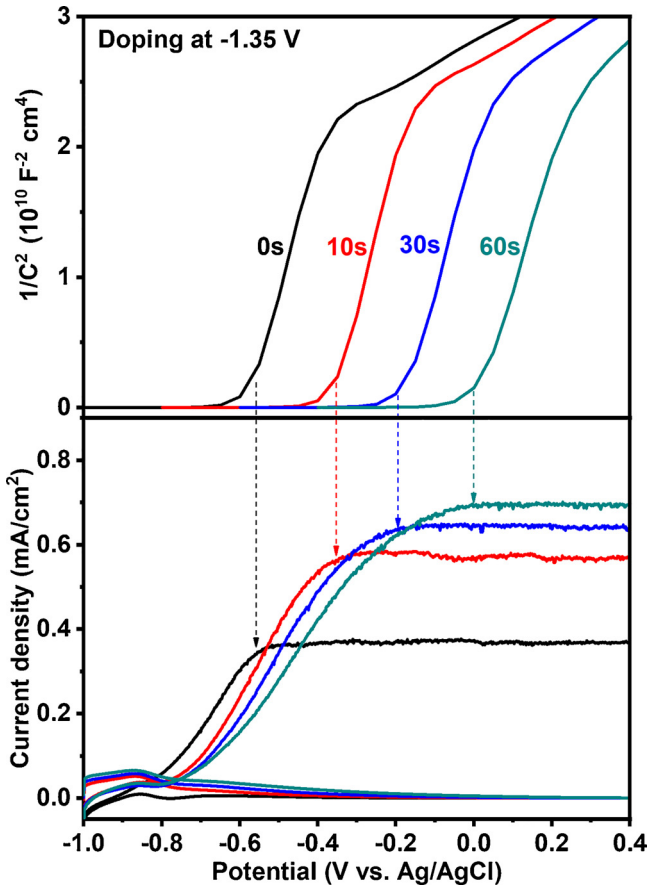

Fig. 1. The correlation of Mott-Schottky plots (top) and photocurrent density curves (bottom) of TiO_2 nanotubes electrode after electrochemical doping in 1 M NaOH solution at -1.35 V for 0, 10, 30, and 60 s.

system [35].

3. Results and discussion

To enlarge the surface effect, the TiO_2 nanotubes were synthesized by electrochemical anodic oxidation with heating treatment at 450 °C for 2 h, and a subsequent electrochemical doping treatment at -1.35 V. X-ray diffraction (XRD) pattern revealed that the as-prepared samples before and after electrochemical doping, were crystallized single-phase TiO_2 with anatase structure (JCPDS Card No. 21–1272) (Fig. S1). Scanning electron microscope (SEM) observations indicated that the TiO_2 film is composed of uniform nanotubes with 90–100 nm in diameter, about 10-20 nm in thickness of tube wall and 5-6 μm in length (Fig. S2 and S3). The average *d* spacing estimated from the lattice fringe in the high-resolution transmission electron microscope (TEM) image is 0.33 nm, well consistent with the anatase (101) plane (Fig. S4). The morphologies and structures of the TiO_2 nanotubes were almost not varied after electrochemical doping.

The photocurrent on the TiO_2 nanotube photoanodes was recorded in 1 M NaOH solution under a 500 W Xe lamp irradiation (Fig. 1). Prolonging the electrochemical doping time, the saturated photocurrent significantly increased. And clearly, although the TiO_2 nanotube photoanodes exhibited the similar onset potential at about -0.8 V, the external applied potentials at which photocurrent saturation increased with increase of electrochemical doping times. UV–vis absorption spectra revealed that the electrochemical doping does not change the main band edge of TiO_2 nanotube phoanodes to be at 380 nm (Fig. S5). The photocurrent recorded under the irradiation *via* a band-pass filter confirmed that the photocurrent completely originated from the band-band excitation (Fig. S6). Therefore, the increased photocurrent density would be attributed to the improved charge separation efficiency or the accelerated interface reaction kinetics. A slight photocurrent difference was observed at the electrolyte with or without Na_2SO_3 hole scavenger (Fig. S7), indicating that the electrochemical doping does not change the OER kinetics. Therefore, we believe that the PEC performance of TiO_2 nanotubes electrode is mainly promoted by the charge separation efficiency.

In principle, the photocurrent will occur at the flat band potential (U_{fb}) of semiconductor [36]. For a plate electrode, the U_{fb} can be determined by the intercept of tangent line of Mott-Schottky (M–S) relationship on potential axis. The classic M–S relationship derived from the plate electrode model is described as $\left(\frac{1}{C}\right)^2 = \frac{2}{qk\varepsilon_0 N_d}(V - V_{fb} - \frac{k_B T}{q})$, where C is the capacitance per unit surface area, V is applied voltage, N_d is the donor density, k_B is the Boltzmann constant, T is the absolute temperature, q is the elementary charge, κ is the dielectric constant of the semiconductor, ε_0 is the vacuum permittivity. In the case of TiO_2 nanotubes electrode, the M–S measurement in 1 M NaOH at 1 kHz exhibited three linear ranges (Figs. 1 and 2 a). In the previous reports [18,21,37–40], the intercept of tangent line for the second linear range of M–S relationship on potential axis usually is assigned to the U_{fb} of

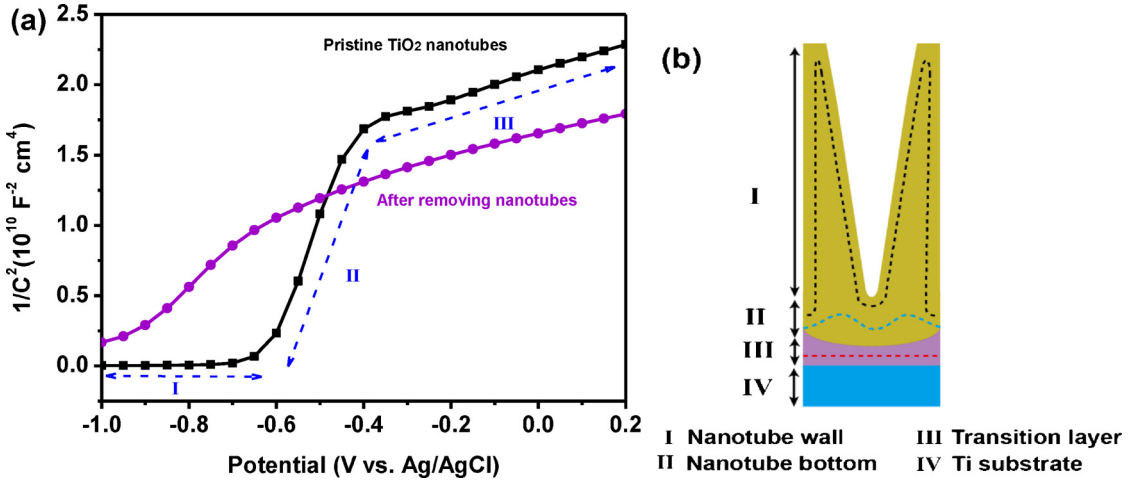

Fig. 2. (a) Mott-Schottky plots for TiO_2 electrodes in the dark in 1 M NaOH electrolyte at 1 kHz. (b) A schematic diagram to show TiO_2 nanotube electrode structure and the boundary (broken line) between the depletion layer and neutral region when applying different bias on the TiO_2 nanotube electrodes. -1 V ~ -0.6 V: black broken line; -0.6 V ~ -0.4 V: blue broken line; > -0.4 V: red broken line (For interpretation of the references to colour in this figure legend, the reader is referred to the web version of this article).

TiO_2. However, in our case, the intercept corresponds to the potential at which photocurrent saturation of TiO_2 nanotube photoanodes and shifts positively when prolonged the electrochemical doping times (Fig. 1). Evidently, these intercepts from the second linear M–S regions are all positive than photocurrent onset potentials. The clear discrepancy means that the M–S relationship of TiO_2 nanotubes electrode is complicated and is not fully understood.

After annealing, the electrode is composed of TiO_2 nanotube wall, TiO_2 nanotube bottom, and a transition layer between TiO_2 nanotube bottom and Ti substrate. To assign the nature of M–S plot, the nanotubes were removed from the Ti substrate. SEM observation revealed that after removing the nanotubes the transition layer presents small honeycomb surface (Fig. S8a). The M–S plot for the electrode after removing the nanotube layer, which would reflect the capacitance behaviors of the transition layer, is nearly single linear M–S relationship and shares the same slope with the third linear range of the M–S plot for the TiO_2 nanotubes electrode (Fig. 2a). This fact means that the third linear range of the M–S relationship of the TiO_2 nanotubes electrode occurring at high bias ranges (-0.4 to 0.2 V) describes the capacitance behaviors of the transition layer. Indeed, a similar phenomenon, the capacitance behavior of indium tin oxide (ITO) substrate, was observed when the space charge layer of TiO_2 on TiO_2/ITO was fully depleted by high bias [41].

According to the classic M–S equation derived from the plate electrode model, the differential capacitance equals the product of the capacitance per unit surface area and the surface area of the boundary between the depleted and the neutral parts of the semiconductor [42]. However, in our case, the geometric projection area, which is far lower than the actual boundary area between the depleted and the neutral part of nanotube, is used to describe the M–S relationship. Therefore, the first linear M–S region (-1.0 to -0.6 V) with a small slope can be assigned to the depletion layer capacitance behavior of the TiO_2 nanotube wall due to that the M–S calculation based on the electrode geometric projection area in place of large nanotube wall surface area will produce the small slope. At low bias the band bending is slight and the depletion layer is so thin underneath the surface of the nanotube wall (Fig. 2b). The width of the depleted region increases as the bias is increased. Once the entire nanotube wall is depleted (at -0.6 V), it no longer contributes to the differential capacitance [42]. Then, the second linear M–S region (-0.6 to -0.4 V) occurs and can be ascribed to the capacitance behavior of the TiO_2 nanotube bottom due to its thick bulk feature (Fig. S8c, about 80 nm) compared to the about 10–20 nm TiO_2 nanotube wall, requiring higher bias to deplete charge carriers. Subsequently, the charge carriers at transition layer initials to deplete at higher bias (third linear M–S region, above -0.4 V). The boundary between the depleted and the neutral part of both the nanotube bottom region and the transition layer is nearly planar (Fig. 2b). However, the slope of the second M–S region is larger than that of the third region, that is, the carrier concentration in nanotube bottom region is lower than that in the transition layer. This probably resulted from the less defects for nanotube bottom region than transition layer due to that the oxygen diffusion into the transition layer is not sufficient during annealing (Fig. S9).

These evidences indicated that the M–S plot of TiO_2 nanotube electrode was complicated due to its complex nanostructure interfaces, and was not suitable to use it to determine the flat band potential of TiO_2. The main deviation resulted from that the use of unreal surface area greatly affected the slope of linear range of M–S relationship. The different bias requirement for charge depletion on the different curved surfaces also induced that it is more difficult to distinguish the complex capacitance information.

Next, we would like to explore the nature of the electrochemical doping induced both the positive shift of M–S plot and the saturated photocurrent enhancement with prolonging the doping times. Obviously, electrochemical doping greatly affected the M–S relationship of TiO_2 nanotubes electrode. It has been well demonstrated that applying a high negative bias enables protons to insert into the surface lattice of TiO_2 [43]. This implies that the electrochemical doping will change the surface compositions of TiO_2 nanotubes, thus the surface capacitance. Indeed, the potential requirement for charge depletion in the nanotube wall (first M–S region) gradually increased from -0.6 to -0.2 V when varied doping times from 0 to 60 s (at -1.35 V), indicating that the electrochemical doping enlarges the surface capacitance of the TiO_2 nanotube wall. It seems reasonable to conclude that the electrochemical doping introduced the surface states into the TiO_2 nanotube wall. The density of surface states increased with increase of doping times, thus enlarging the surface capacitance of TiO_2 nanotube wall, and requiring the higher bias to deplete. We should know that when the nanotube wall was depleted so was the surface state on the nanotube wall, which cannot be distinguished because of the equal capacitance of the surface state and the space charge layer collected in parallel [2,44]. The potential window for M–S plot of TiO_2 nanotube wall narrows with increasing the measured frequency (Fig. S10), implying the amounts of charge transfer evidently decreased at the high frequency. It is a typical capacitance behavior of surface states for the slow charge transfer kinetics [45]. The slope of the second M–S region for nanotube bottom was not changed after electrochemical doping (Fig. 1). Therefore, we believe that carrier concentration in the bulk of TiO_2 nanotube was not changed after electrochemical doping. The increased applied potential to deplete the nanotube wall (first M–S region) is mainly contributed by the increased surface state density. The potential window for charge depletion decays to above 0.6 V on an overdoped TiO_2 nanotube wall obtained at the -1.5 V for 10 s (Fig. S11a), further confirming that the capacitance behavior is dependent on the charge transfer amount and transfer kinetics. Interestingly, for all TiO_2 nanotube electrodes with or without electrochemical doping, the potential required for complete depletion of nanotube wall is the same as that for photocurrent reaching saturation. This probably means that the complete depletion of surface states on TiO_2 nanotube wall is positive relation to the highest charge separation efficiency.

Diffuse reflection using Fourier transform spectroscopy (DRIFTS) and X-ray photoelectron spectroscopy (XPS) analyses were carried out to check the surface compositions of TiO_2 nanotubes after electrochemical doping. The DRIFTS signals (Fig. 3a) ranging from 3200 to 3800 cm^{-1} are assigned to the stretching mode of -OH groups and peak signal around 1600 cm^{-1} was ascribed to stretching mode of a surface coordinated water species [46–49]. Their transmittance intensities significantly decreased when the TiO_2 nanotubes were overdoped at -1.8 V for 60 s, confirming that the electrochemical doping increases the amounts of -OH groups. The DRIFTS signals smaller than 1000 cm^{-1} are attributed to Ti-O stretching mode for anatase [50,51]. Obviously, the transmittance intensity of Ti-O stretching mode did not change when varied electrochemical doping potential or potential holding time, indicating that the increased amounts of -OH groups mainly occurs at the surface of TiO_2 nanotube wall.

XPS survey spectrum displayed that there are only Ti and O XPS signals for the TiO_2 nanotubes after electrochemical doping (Fig. S12a). The O1s core-level XPS spectra can be deconvoluted into two peaks (Fig. 3b). The binding energy at 529.8 eV corresponds to lattice oxygen (O_L) in Ti-O bonds of TiO_2. The binding energy at 531.5 eV can be assigned to the oxygen (O_{OH}) in Ti-OH bonds [52,53]. It has been well verified that the electrochemical doping at negative bias enables the protons insert into the lattice of TiO_2 with the reaction of $Ti^{IV}O_2 + e^- + H^+ = Ti^{III}O(OH)$ [43,54]. Indeed, overdoping the TiO_2 nanotubes at -1.8 V for 60 s evidently increased the amount of Ti-OH bonds. The O_{OH}/O atomic ratios increased from 20.3% to 30.3%, in good agreement with the DRIFTS results, further demonstrating that the proton doping occurs. According to Kim et al.'s report, [54] once surface Ti^{IV} sites are reduced and charge compensated by protonation, the paired electron/proton couple (e^-/H^+) can be transferred between adjacent titanium ions localized in the subsurface region of TiO_2 material by a diffusion-like process. However, the diffusion coefficient of protons

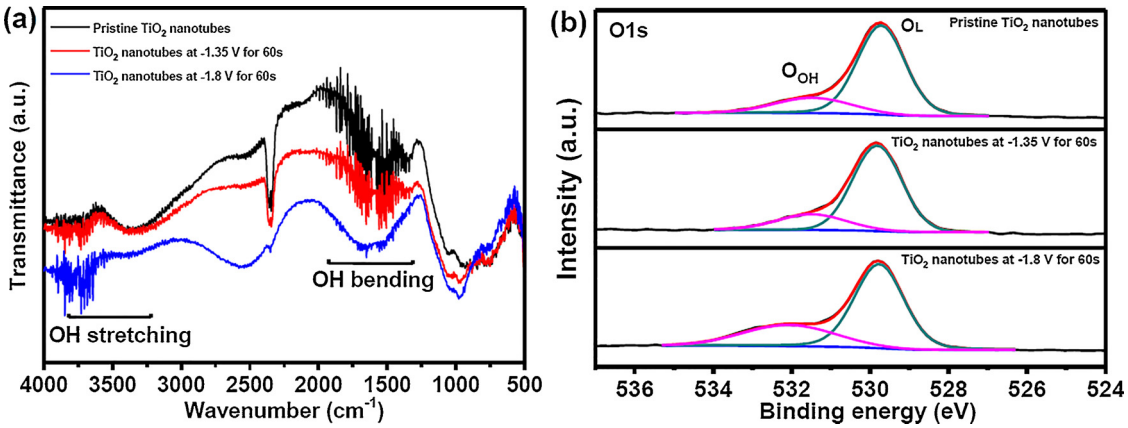

Fig. 3. (a) DRIFTS and (b) XPS spectra of the TiO_2 nanotube electrodes before and after electrochemical doping at -1.35 V for 60 s and overdoping at -1.8 V for 60 s in aqueous 1 M NaOH. The O_{OH}/O atomic ratios were 20.3% for pristine TiO_2 nanotubes, 21.2% for TiO_2 nanotubes at -1.35 V for 60 s, and 30.3% for TiO_2 nanotubes at -1.8 V for 60 s, respectively.

within the metal oxide lattice was very small (10^{-13}-10^{-17} cm^2 s^{-1}). In our case, the doping time is short (60 s), therefore the diffusion length of H^+ within the bulk TiO_2 is expected to be much smaller than the thickness of nanotube wall (about 19 nm). According to the surface information from XPS result, compared to pristine TiO_2 nanotube electrode the O_{OH}/O atomic ratios only slightly increased after TiO_2 nanotube electrode electrochemical doped at -1.35 V for 60 s. This indicated that only a little surface Ti^{IV} sites were reduced, and reduced Ti^{IV} sites in the bulk can be neglected. The UV–vis absorbance spectrum (Fig. S5) and valence band XPS spectra (Fig. S12b) of the TiO_2 nanotubes electrode were almost no variation after electrochemical doping, also proving that the proton doping is a surface reaction process [55].

After inserting the protons into the surface lattice of TiO_2 nanotubes, the photocurrent was significantly improved, suggesting that the surface Ti-OH may act the surface states to promote the charge separation. The optical spectroscopies were used to detect the possible charge trapping by surface states [20,43,54,56,57] Fig. 4a shows the potential-dependent optical absorption spectra of a TiO_2 nanotubes electrode measured in aqueous 1 M NaOH (pH 13.6). An obvious absorption tail in wavelength above TiO_2 band edge of 380 nm was observed when the bias is negative than -1.0 V, which is close to the -1.14 V for U_{fb} of the TiO_2 semiconductor in 1 M NaOH electrolyte (pH 13.6) [44,58]. When the bias is negative than U_{fb}, an accumulation band bending condition will induce the electron filling of available conduction band states and surface states. And the absorption tail significantly goes up with the potential going more negative, demonstrating that the amount of freely moving electron on surface of TiO_2 nanotube wall increased with negative shift of the bias [43,54]. Indeed, the absorption coefficient to increase exponentially with wavelength was observed in the TiO_2 nanotubes at -1.6 V, which was a typical absorption behavior for freely moving electrons [59]. The absorbance of TiO_2 nanotubes at 720 nm is real-time response to the square wave potential oscillating between 0 and -1.6 V, agreement with the surface coloration of TiO_2 nanotubes from light to dark (Fig. 4 b and Video S1), suggesting that the accumulated electrons move freely and quickly. The excess electrons accumulated on TiO_2 surface are able to induce the insertion of protons (H^+) at the electrode/electrolyte interface [43,54]. The trapped electrons will produce an electrostatic field on the surface of TiO_2 nanotube wall, thus attracting the protons or other cations. When the bias is negative than U_{fb} of TiO_2, adding phenolphthalein reagent into the electrolyte, and a red surface of TiO_2 nanotubes is clearly visible due to the local pH increase, confirming that inserting and/or attracting of protons into the lattice and/or on the surface of TiO_2 occurs (Fig. S13a). Such an electrostatic attraction between trapped electrons and counter cations was further verified during the adsorption-desorption process of cationic dye methylene blue (MB) when adjusted the bias more negative than the U_{fb} of TiO_2 (Fig. S13b) [15].

Given that the absorption intensity of freely moving electrons is positive relation to the amount of free electrons, the CV scanning-dependent absorbance spectra were recorded at 720 nm to confirm the electron filling process. To avoid the electrochemical doping, a potential window from -1.0 to 0 V was used. Under nitrogen protection to suppress the oxygen reduction, the exponential increase of current in CVs with a positive-going potential scan would reflect the progressive filling of electronic states that are localized in traps distributed in the band gap f TiO_2, due to that the applied bias is positive than the U_{fb} (-1.14 V at pH 13.6) of TiO_2 [6–8,43,54]. For the pristine TiO_2 nanotubes electrode (Fig. 4c and f), the absorption spectrum during the CV scan period exhibited that the electrons extracted from surface states to be initialed at -1.0 V and fully depleted at potential positive than -0.6 V. Such an electron transfer process is reversible when a negative-going potential scanning was carried out.

During CV scan, absorption intensity of the TiO_2 nanotubes electrode with electrochemical doping at -1.35 V for 60 s strengthened significantly (Fig. 4d and g), indicative of the increased electron transfer number. The electrons trapped in surface states will be not fully depleted during the CV scan period, if TiO_2 nanotubes electrode was overdoped at -1.6 V for 20 s (Fig. 4e and h). These evidences may indicate that the surface states on the TiO_2 nanotubes were the important electron filling places. The increased capacitance by electrochemical doping was further validated by CV scan, electrochemical impedance spectroscopy (EIS) and transient current tests (Fig. S14, S15 and S16), in good agreement with our previous report [14].

After enlarging the electron capacity of surface states by electrochemical doping, the saturated photocurrent of TiO_2 nanotubes electrode enhanced significantly. This may mean that the surface states are an important electron transfer route to promote the charge separation. Here, we use the open-circuit potential (OCP), an equilibrium state to completely avoid the effect of OER reaction kinetics, to check the photogenerated charge separation and transfer (Fig. 5a). In general, the higher the photocurrent would indicate the larger the photovoltage. In this case, under irradiation, the open circuit photovoltage of pristine TiO_2 nanotubes electrode is about 100 and 150 mV larger than those of electrodes with electrochemical doping at -1.35 V for 30 s and 60 s, respectively. After electrochemical doping the surface states density on TiO_2 nanotube increased. This will enhance the Fermi level pinning effect [2,13]. As a result, we observed a lower photovoltage after electrochemical doping. The electron filling capacity of surface states also induced a different decay of the photovoltage upon termination of irradiation. In the previous reports, the decay behavior of the photovoltage under dark was ascribed to reflect the surface charge transfer

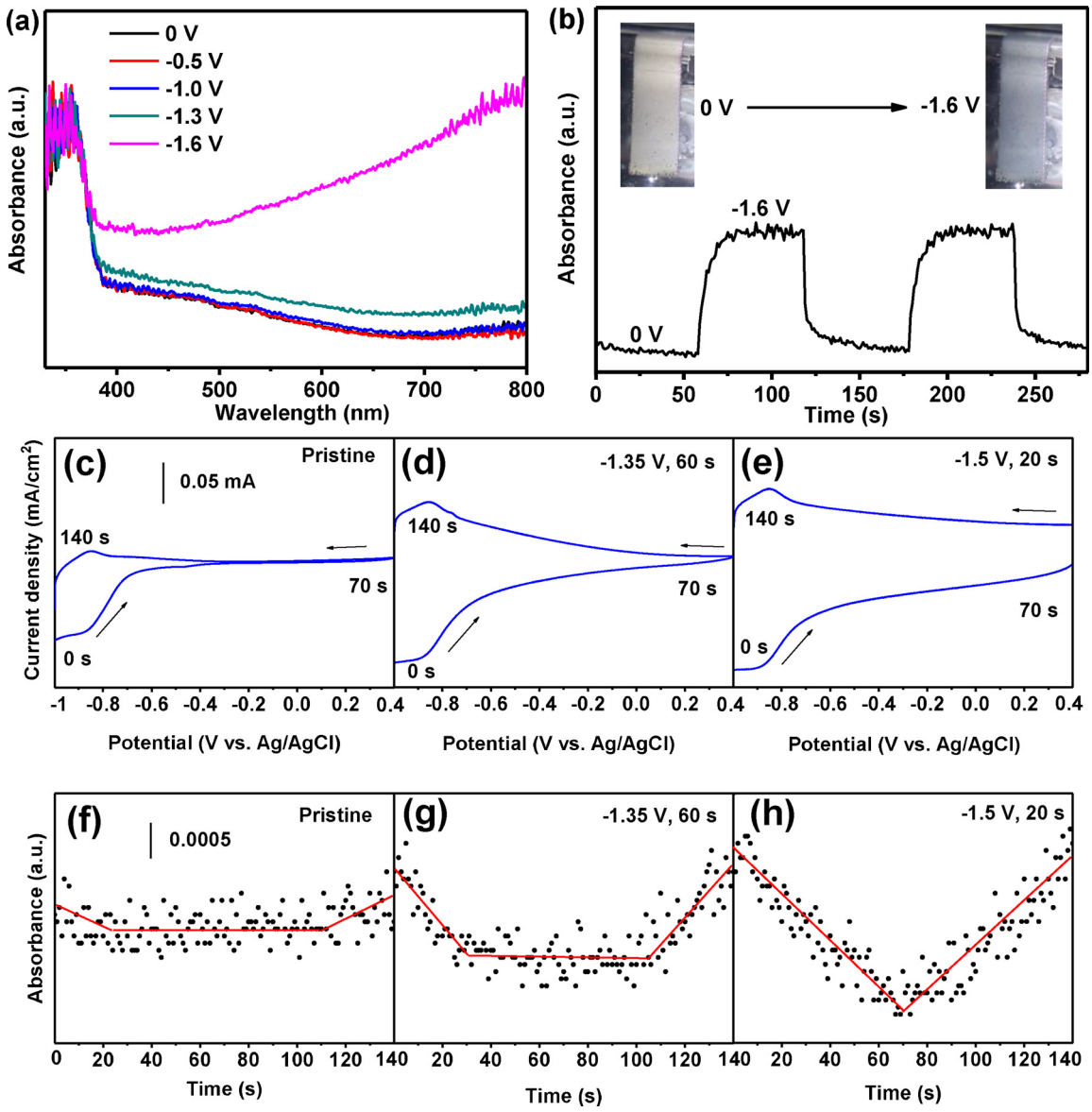

Fig. 4. (a) The UV–vis diffuse reflection spectra of TiO_2 nanotubes electrode in aqueous 1 M NaOH measured at potentials between 0 and -1.6 V. (b) Absorbance at 720 nm for TiO_2 nanotube electrodes in aqueous 1 M NaOH as a function of an applied square wave potential oscillating between 0 and -1.6 V. Inset shows the TiO_2 nanotube electrodes in aqueous 1 M NaOH at applied bias 0 V (left) and -1.6 V (right). (c, d, e) Cyclic voltammograms and (f, g, h) absorbance spectra (monitored at 720 nm) were simultaneously recorded in aqueous 1 M NaOH. Pristine TiO_2 nanotubes (c, f), electrochemical doping at -1.35 V for 60 s (d, g), electrochemical doping at -1.6 V for 20 s (e, h). Electrodes were scanned from -1 to 0.4 V at a scan rate 20 mV s^{-1}.

and recombination kinetics, that is, the electrons accumulated within the TiO_2 are scavenged by the electron acceptor species in the electrolyte as well as undergo recombination with trapped holes [20,23,40,60,61]. In our case, obviously, the photovoltage decay times were prolonged with increasing the surface state density, meaning that the electron capacity of surface states are also an important factor to affect the photovoltage decay due to the slow charge transfer and recombination kinetics. Therefore, in the case of TiO_2 nanotubes electrode, the prolonged decay time would result from the increased amount of electrons trapped in surface states and the slow surface charge transfer and recombination kinetics.

We use the resistor-capacitor equivalent circuit model (Fig. 5b) to fit the photovoltage decay curve by formula of $\frac{E-E_{ph}}{E_o-E_{ph}} = 1-\exp(\frac{-t}{R_{ct}C_{trap}})$, where E represents OCP at any time, E_o represents the dark stable OCP value, E_{ph} represents the stable OCP value under illumination, C_{trap} is the surface state capacitance, R_{ct} is charge transfer resistance. The decay time constant $\tau = R_{ct}C_{trap}$ can be calculated by the mentioned-above formula fitting to data. For TiO_2 nanotubes electrode after electrochemical doping, the calculated τ exhibited about 2.5 times increase, the C_{trap} can be estimated from the CV scan (Fig. S17) and presented about 3 times increase, and R_{ct} can be obtained by $\tau = R_{ct}C_{trap}$ and gives about 0.3 times decrease. This means that, for the TiO_2 nanotubes electrode with or without elelctrochemiucal doping, they have the similar charge transfer and recombination kinetics. The τ increase is mainly contributed by C_{trap}, that is, the amount of electron trapped in surface states. An electrochemical polarization in the dark for 60 s was carried out by using illuminated stead-state OCP as a bias, then switch to OCP mode quickly to monitor the voltage decay as a function of time. We find an interesting phenomenon that the OCP decay after electrochemical (EC) polarization was almost the same as that for PEC and their time constants τ were very similar (Fig. 5c and S18). It indicated that both the photogenerated electrons and the conduction band electrons are able to relax into the surface states. The charge transfer kinetics evidently improved by adding of H_2O_2 into 1 M NaOH electrolyte

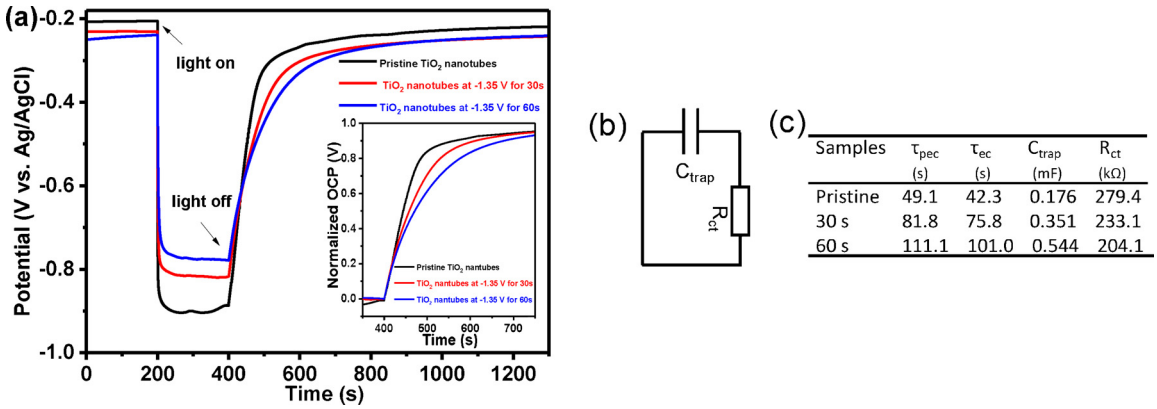

Samples	τ_{pec} (s)	τ_{ec} (s)	C_{trap} (mF)	R_{ct} (kΩ)
Pristine	49.1	42.3	0.176	279.4
30 s	81.8	75.8	0.351	233.1
60 s	111.1	101.0	0.544	204.1

Fig. 5. (a) The open-circuit potential (OCP) under light on and off in aqueous 1 M NaOH on the as-obtained electrode and the electrodes that were respectively electrochemically doped at -1.35 V for 30 s and 60 s in 1 M NaOH. Inset shows the normalized OCP curves after turning off the light. (b) Equivalent circuit used to simulate photovoltage decay process and (c) parameters obtained by fitting the OCP curves.

because H_2O_2 is a strong electron acceptor (Fig. S19), confirming that the electron transfer kinetics is mainly affected by electron acceptor species in the electrolyte and is weakly dependent on the electrochemical doping.

The density functional theory (DFT) calculations were performed to understand the nature of electron storage in surface states, Ti-OH species. Anatase (101) surface model (Fig. S20), a most stable facet for anatase TiO_2, was constructed to calculate charge redistribution after hydrogen bonded with surface bridging oxygen atom (O_b) (Fig. 6a). The calculated charge density differences showed that the surface covered with H atoms increases the charge density on the bridging O atoms, as well as on the six coordinate Ti_{6c}^{4+} ions (Fig. 6b). The calculated results indicated that upon chemisorption of H atoms there is a partial electron transfer to the Ti 3d orbitals. Bader charge analysis revealed that about 0.67 electrons were transferred from H into Ti-O during inserting H to form Ti-OH. This conclusion is consistent with the studies of H atoms or alkali atom chemisorption on rutile [62]. After electrochemical doping, the downshifting of baseline of DRIFTS (Fig. 3a), is interpreted as evidence of the presence of the free charge carriers that decrease the infrared reflectivity of TiO_2 surfaces [48,49]. This would indicate that when the Ti-OH structure formed on the TiO_2 surface the electrons from H atoms will stabilize in the Ti-OH surface states and then be extracted through available conduction band states to the external circuit by applying positive bias on the TiO_2 nanotube electrodes. When used a negative potential, the electrons from external circuit will return to the surface states to make the system electrically neutral.

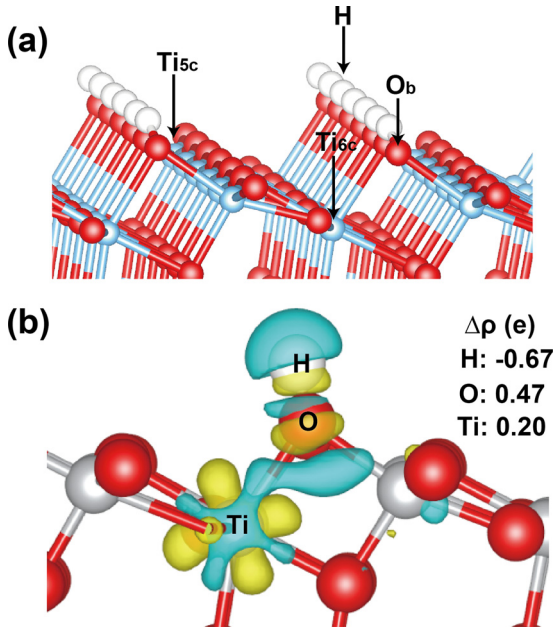

Fig. 6. (a) A slab model of anatase (101) surface with H absorbed on the bridge O (O_b) atom. White, Red, and green spheres indicate the hydrogen, titanium, and oxygen atoms, respectively. (b) Charge density difference for one H atom absorbed on the bridge O atom of anatase (101) surface. The yellow and green charge densities correspond to charge accumulation and depletion, respectively. The electron transfer number (Δρ) was obtained by Bader charge analysis (For interpretation of the references to colour in this figure legend, the reader is referred to the web version of this article).

Now we can understand the charge transfer process happening on TiO_2 nanotube electrodes during photoelectrochemical water splitting reaction under illumination. In the dark, applying positive bias on the TiO_2 nanotube electrodes until both the depletion layer of nanotube walls and the surface states were depleted, all the electrons trapped in Ti^{III}-OH will be extracted through available conduction band states to the external circuit. The excess positive charges remain on the surface of the nanotube to be stabilized by formation of Ti^{IV}-OH *via* a reaction of Ti^{III}-OH - e_{cb}^- = Ti^{IV}-OH. Once the light illuminated on the electrode the photogenerated electrons will be captured by the Ti^{IV}-OH *via* a reaction of Ti^{IV}-OH + e_{ph}^- = Ti^{III}-OH before recombining with photogenerated holes (Fig. 7a), and then the electrons in Ti^{III}-OH will be extracted *via* available conduction states to the external circuit ($Ti^{III}OH$ - e_{cb}^- = $Ti^{IV}OH$), leading to the generation of long lived holes. These long lived holes go on to drive water oxidation [63].

The similar decay time constant of OCP curves for PEC and EC processes (Fig. S18) is also a result of transferring the electrons in conduction band states into electrolyte *via* the Ti^{III}-OH surface states [14,48,64].The photocurrent density will reach the maximum at the potential the Ti^{III}-OH surface states fully depleted. Before reaching to the potential at which photocurrent saturation, with the increase of the positive-going bias, more surface states were depleted and more photogenerated electrons can be trapped into it. Until the entire surface states were depleted, the photocurrent density got saturated due to that a steady-state filling and extraction process of surface state electrons was built. Electrochemical doping much more Ti^{III}-OH on the TiO_2 nanotube surface greatly increased the surface state density and more positive potential was needed to fully depleted the surface states. As a result, we observed a higher saturated photocurrent density at a more positive potential.

These mentioned-above evidences indicated that the surface states are an important electron transfer route, which enhance the charge lifetime and charge separation efficiency. Noting that the photocurrent density of TiO_2 photoanodes got saturated quickly and is independent of the applied bias positive than the potential at which photocurrent saturation [29,38,52,65,66] indicating that at which potentials

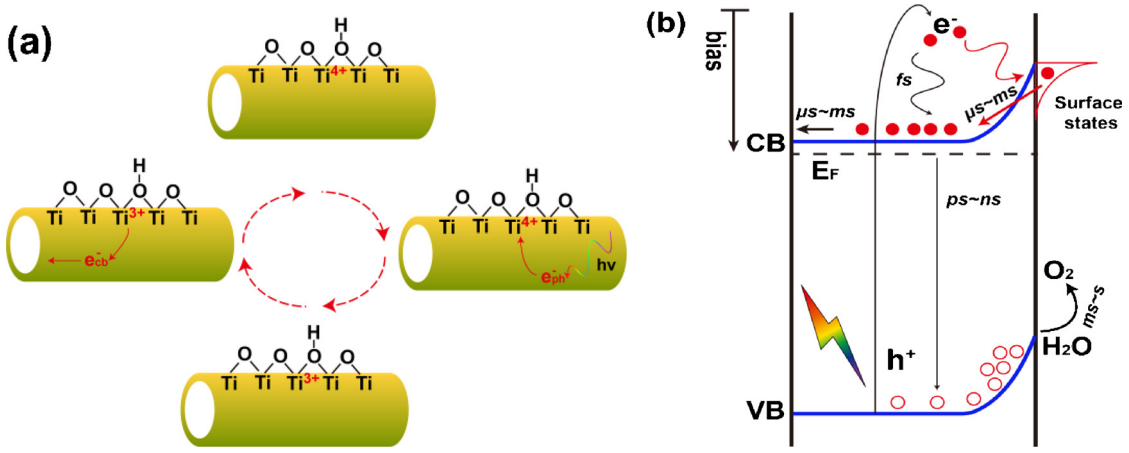

Fig. 7. Possible mechanisms for photoelectron separation and transfer on a TiO_2 nanotube surface. (a) The trapping and detrapping a photogenerated electron into/from surface states. (b) Under illumination and external potential bias, the charge transfer processes and corresponding time scales.

increasing the applied bias almost did not retard the electron-hole recombination kinetics in the depletion region of TiO_2 photoanode. This fact suggested that an equilibrium state, among charge separation in depletion region, charge relaxing to conduction or surface states, and charge extracting to external circuit, was built quickly in TiO_2 electrodes. This would be attributed to that before occurrence of saturated photocurrent both the depletion region and surface states are greatly sensitive to the changes of applied bias, probably due to the small charge effective mass in TiO_2 [67]. As described in Fig. 7b, in the depletion region, most of the photogenerated electrons recombined with the holes on *ps* or *ns* scale [68–70], before extracted to the external circuit (on *μs*∼*ms*) [69]. The saturated photocurrent was mainly limited by the charge recombination in depletion region if there is no surface states on the electrodes, also probably by the charge recombination in the surface states if the surface states act as a recombination center. At this case, the saturated photocurrent cannot be observed even at a high applied bias [63]. Indeed, the yield of long-lived holes is quantitative correlation to the photocurrent, and is dependent on retarding the electron-hole recombination in depletion region of Fe_2O_3 by applied bias [11,16,71–73]. Here, we have demonstrated that the electrons trapped in surface states of TiO_2 exhibited a long-lived time. When introduced the surface states, the surface states Ti-OH on the nanotube can trap and stabilize the photogenerated electrons before their recombination with holes. Electrons trapped in the surface states are extracted to the external circuit in the time scale of *μs*∼*ms*, which can be estimated from M–S plots (Fig. S10). These evidences mean that surface states Ti-OH on the TiO_2 nanotube increase charge separation efficiency *via* changing the electron transfer route, contributing to the PEC performance enhancement.

We can expect that if the TiO_2 nanotube electrode were overdoped so that at the potential window used in this study the surface states could not be fully depleted, the photocurrent density will increase gradually with the applied bias but no saturated photocurrent occurred. The result showing the photocurrent-potential curve of a TiO_2 nanotube electrode with overdoping at -1.5 V for 10 s confirmed this sequitur (Fig. S11b). It seems reasonable to infer that the pH values of electrolyte will affect the formation of surface states, thus influence the saturated photocurrent. The saturated photocurrent of pristine TiO_2 nanotubes electrode measured in aqueous 0.5 M H_2SO_4 is evidently higher than that measured in 1 M NaOH (Fig. S21 and S22). In acidic electrolyte, the surface of the TiO_2 nanotubes electrode was covered by the Ti-OH and Ti-OH_2 species due to the protonated and deprotonated effect [46,47]. As a result, the surface states density was increased like the TiO_2 nanotubes electrode after electrochemical doping treatment. The CV scan indicated that the capacitance of pristine TiO_2 nanotubes electrode is significantly increased for measured in acidic electrolyte than in basic electrolyte (Fig. S22b). The M–S plot of TiO_2 nanotube wall is pH-dependent (Fig. S22d). The increase step of initial potential at which the nanotube walls and surface states fully depleted is about 74 mV per pH, is 15 mV higher than the ∼59 mV per pH for theoretical U_{fb} of TiO_2 described by the Nernst equation. This probably resulted from that the density of the surface states increased with the concentration of the H^+ ions in the electrolyte.

4. Conclusions

In this work, we have made a possible explanation for the M–S plot of TiO_2 nanotubes electrode and demonstrated that the surface states, Ti-OH species, are the important photogenerated electron transfer route. The enhancement of the PEC performance of the TiO_2 nanotubes electrode after electrochemical doping protons into the lattice of TiO_2 were not attributed to the passivation of the trap states, but the increased surface state density, which can capture photogenerated electrons before they recombined with photogenerated holes, hence increasing the charge separation efficiency. Our results offer a new insight to understanding the role of surface states during the charge separation, transfer, and injection processes of the water splitting reaction.

Acknowledgment

This work was supported primarily by the National Basic Research Program of China (2013CB632404), the National Natural Science Foundation of China (51572121, 21603098, and 21633004), the Natural Science Foundation of Jiangsu Province (BK20151265, BK20151383, and BK20150580), the program B for Outstanding PhD candidate of Nanjing University (201702B084), the Postdoctoral Science Foundation of China (2017M611784), the State Key Laboratory of NBC Protection for Civilian (SKLNBC2014-09), and the Fundamental Research Funds for the Central Universities (021314380084). We are grateful to the High Performance Computing Center (HPCC) of Nanjing University for doing the numerical calculations in this paper on its IBM Blade cluster system.

Appendix A. Supplementary data

Supplementary material related to this article can be found, in the online version, at doi:https://doi.org/10.1016/j.apcatb.2018.04.040.

References

[1] J.H. Montoya, L.C. Seitz, P. Chakthranont, A. Vojvodic, T.F. Jaramillo,

J.K. Nørskov, Nat. Mater. 16 (2017) 70–81.
[2] A.J. Bard, A.B. Bocarsly, F.R.F. Fan, E.G. Walton, M.S. Wrighton, J. Am. Chem. Soc. 102 (1980) 3671–3677.
[3] A.L. Linsebigler, G. Lu, J. John, T. Yates, Chem. Rev. 95 (1995) 735–758.
[4] A. Fujishima, X. Zhang, D.A. Tryk, Surf. Sci. Rep. 63 (2008) 515–582.
[5] T.L. Thompson, J.T. Yates, Chem. Rev. 106 (2006) 4428–4453.
[6] H. Wang, J. He, G. Boschloo, H. Lindström, A. Hagfeldt, S.E. Lindquist, J. Phys. Chem. B 105 (2001) 2529–2533.
[7] L. Bertoluzzi, I. Herraiz-Cardona, R. Gottesman, A. Zaban, J. Bisquert, J. Phys. Chem. Lett. 5 (2014) 689–694.
[8] M. Jankulovska, T. Berger, S.S. Wong, R. Gómez, T. Lana-Villarreal, ChemPhysChem 13 (2012) 3008–3017.
[9] K. Sivula, J. Phys. Chem. Lett. 4 (2013) 1624–1633.
[10] F. Le Formal, S.R. Pendlebury, M. Cornuz, S.D. Tilley, M. Gra, J.R. Durrant, J. Am. Chem. Soc. 136 (2014) 2564–2574.
[11] B. Klahr, S. Gimenez, F. Fabregat-Santiago, T.W. Hamann, J. Am. Chem. Soc. 134 (2012) 4294–4302.
[12] M. Green, J. Chem. Phys. 31 (1959) 200–203.
[13] J.E. Thorne, S. Li, C. Du, G. Qin, D. Wang, J. Phys. Chem. Lett. 6 (2015) 4083–4088.
[14] H. Zhu, S. Yan, Z. Li, Z. Zou, ACS Appl. Mater. Interfaces 9 (2017) 33887–33895.
[15] T. He, L. Wang, F. Fabregat-Santiago, G. Liu, Y. Li, C. Wang, R. Guan, J. Mater. Chem. A 5 (2017) 6455–6464.
[16] F. Le Formal, K. Sivula, M. Grätzel, J. Phys. Chem. C 116 (2012) 26707–26720.
[17] F. Fabregat-Santiago, E.M. Barea, J. Bisquert, G.K. Mor, K. Shankar, C.A. Grimes, J. Am. Chem. Soc. 130 (2008) 11312–11316.
[18] H. Zhou, Y. Zhang, J. Phys. Chem. C. 118 (2014) 5626–5636.
[19] H. Wu, D. Li, X. Zhu, C. Yang, D. Liu, X. Chen, Y. Song, L. Lu, Electrochim. Acta 116 (2014) 129–136.
[20] B.H. Meekins, P.V. Kamat, ACS Nano 3 (2009) 3437–3446.
[21] W. Liao, J. Yang, H. Zhou, M. Murugananthan, Y. Zhang, Electrochim. Acta 136 (2014) 310–317.
[22] C. Kim, S. Kim, J. Choi, J. Lee, J.S. Kang, Y.E. Sung, J. Lee, W. Choi, J. Yoon, Electrochim. Acta 141 (2014) 113–119.
[23] L. Tsui, M. Saito, T. Homma, G. Zangari, J. Mater. Chem. A. 3 (2015) 360–367.
[24] G. Wang, Y. Yang, Y. Ling, H. Wang, X. Lu, Y.C. Pu, J.Z. Zhang, Y. Tong, Y. Li, J. Mater. Chem. A. 4 (2016) 2849–2855.
[25] L. Tsui, Y. Xu, D. Dawidowski, D. Cafiso, G. Zangari, J. Mater. Chem. A. 4 (2016) 19070–19077.
[26] C. Kim, S. Kim, S.P. Hong, J. Lee, J. Yoon, Phys. Chem. Chem. Phys. 18 (2016) 14370–14375.
[27] S. Wang, P. Chen, J. Yu, Y. Hu, L. Wang, Angew. Chem. Int. Ed. 56 (2017) 8500–8504.
[28] J.M. Jimenez Morales, G.R. Bourret, T. Berger, K.P. McKenna, J. Am. Chem. Soc. 138 (2016) 15956–15964.
[29] Q. Liu, J. He, T. Yao, Z. Sun, W. Cheng, S. He, Y. Xie, Y. Peng, H. Cheng, Y. Sun, Y. Jiang, F. Hu, Z. Xie, W. Yan, Z. Pan, Z. Wu, S. Wei, Nat. Commun. 5 (2014) 5122.
[30] J.P. Perdew, K. Burke, M. Ernzerhof, Phys. Rev. Lett. 77 (1996) 3865–3868.
[31] J.P. Perdew, Y. Wang, Phys. Rev. B 46 (1992) 947–954.
[32] G. Kresse, J. Hafner, Phys. Rev. B 47 (1993) 558–561.
[33] G. Kresse, J. Hafner, Phys. Rev. B 48 (1993) 13115–13118.
[34] H.J. Monkhorst, J.D. Pack, Phys. Rev. B 13 (1976) 5188–5192.
[35] R.F.W. Bader, Atoms in Molecules. Encyclopedia of Computational Chemistry, John Wiley & Sons, Ltd, Chichester, U.K, 2002.
[36] M. Jankulovska, T. Berger, T. Lana-Villarreal, R. Gómez, Electrochim. Acta 62 (2012) 172–180.
[37] Z. Zhang, M.N. Hedhili, H. Zhu, P. Wang, Phys. Chem. Chem. Phys. 15 (2013) 15637–15644.
[38] H. Li, J. Chen, Z. Xia, J. Xing, J. Mater. Chem. A. 3 (2015) 699–705.
[39] Y. Yang, J. Liao, Y. Li, X. Cao, N. Li, C. Wang, S. Lin, RSC Adv. 6 (2016) 46871–46878.
[40] H. Kim, D. Monllor-Satoca, W. Kim, W. Choi, Energy Environ. Sci. 8 (2015) 247–257.
[41] R. van de Krol, A. Gossens, J. Schoonman, J. Electrochem. Soc. 144 (1997) 1723–1727.
[42] B.H. Erné, J. Electrochem. Soc. 143 (1996) 305–314.
[43] G. Boschloo, D. Fitzmaurice, J. Phys. Chem. B 103 (1999) 7860–7868.
[44] G. Rothenberger, D. Fitzmaurice, M. Grätzel, J. Phys. Chem. 96 (1992) 5983–5986.
[45] S. Roy Morrison, Electrochemistry at Semiconductor and Oxidized Metal Electrodes, Plenum, New York, 1980, pp. 132–133.
[46] M. Minella, M.G. Faga, V. Maurino, C. Minero, E. Pelizzetti, S. Coluccia, G. Martra, Langmuir 26 (2010) 2521–2527.
[47] P.A. Connor, K.D. Dobson, A.J. Mcquillan, LAngmuir 15 (1999) 2402–2408.
[48] S.H. Szczepankiewicz, A.J. Colussi, M.R. Hoffmann, J. Phys. Chem. B 104 (2000) 9842–9850.
[49] D.A. Panayotov, J.T. Yates, Chem. Phys. Lett. 410 (2005) 11–17.
[50] Z.W. Qu, G.J. Kroes, J. Phys. Chem. B 110 (2006) 8998–9007.
[51] Y. Kakuma, A.Y. Nosaka, Y. Nosaka, Phys. Chem. Chem. Phys. 17 (2015) 18691–18698.
[52] T. Zhang, S. Cui, B. Yu, Z. Liu, D. Wang, Chem. Commun. 51 (2015) 16940–16943.
[53] B. Erdem, R.A. Hunsicker, G.W. Simmons, E.D. Sudol, V.L. Dimonie, M.S. El-Aasser, Langmuir 17 (2001) 2664–2669.
[54] Y.S. Kim, S. Kriegel, K.D. Harris, C. Costentin, B. Limoges, V. Balland, J. Phys. Chem. C 121 (2017) 10325–10335.
[55] X. Chen, L. Liu, P.Y. Yu, S.S. Mao, Science 331 (2011) 746–751.
[56] B.O. Regan, M. Grätzel, D. Fitzmaurice, Chem. Phys. Lett. 183 (1991) 89–93.
[57] B.O. Regan, M. Grätzel, D. Fitzmaurice, J. Phys. Chem. 95 (1991) 10525–10528.
[58] J.M. Bolts, M.S. Wrighton, J. Phys. Chem. 80 (1976) 2641–2645.
[59] U. Kolle, J. Moser, M. Grätzel, Inorg. Chem. 24 (1985) 2253–2258.
[60] C. Ding, Z. Wang, J. Shi, T. Yao, A. Li, P. Yan, B. Huang, C. Li, ACS Appl. Mater. Interfaces 8 (2016) 7086–7091.
[61] J. Xiao, H. Huang, Q. Huang, L. Zhao, X. Li, X. Hou, H. Chen, Y. Li, J. Catal. 350 (2017) 48–55.
[62] J. Zhao, B. Li, K.D. Jordan, J. Yang, H. Petek, Phys. Rev. B 73 (2006) 195309.
[63] S.R. Pendlebury, A.J. Cowan, M. Barroso, K. Sivula, J. Ye, M. Grätzel, D.R. Klug, J. Tang, J.R. Durrant, Energy Environ. Sci. 5 (2012) 6304–6312.
[64] S.H. Szczepankiewicz, J.A. Moss, M.R. Hoffmann, J. Phys. Chem. B 106 (2002) 7654–7658.
[65] D. Wang, L. Liu, F. Zhang, K. Tao, E. Pippel, K. Domen, Nano Lett. 11 (2011) 3649–3655.
[66] T. Zhang, Y. Liu, J. Liang, D. Wang, Appl. Surf. Sci. 394 (2017) 440–445.
[67] H. Tang, R. Sanjinès, P.E. Schmid, F. Lévy, J. Appl. Phys. 75 (1994) 2042–2047.
[68] A.J. Cowan, C.J. Barnett, S.R. Pendlebury, M. Barroso, K. Sivula, M. Grätzel, J.R. Durrant, D.R. Klug, J. Am. Chem. Soc. 133 (2011) 10134–10140.
[69] A. Kafizas, Y. Ma, E. Pastor, S.R. Pendlebury, C. Mesa, L. Francàs, F. Le Formal, N. Noor, M. Ling, C. Sotelo-Vazquez, C.J. Carmalt, I.P. Parkin, J.R. Durrant, ACS Catal. 7 (2017) 4896–4903.
[70] A.J. Cowan, J. Tang, W. Leng, J.R. Durrant, D.R. Klug, J. Phys. Chem. C 114 (2010) 4208–4214.
[71] H. Dotan, K. Sivula, M. Grätzel, A. Rothschild, S.C. Warren, Energy Environ. Sci. 4 (2011) 958–964.
[72] C. Du, X. Yang, M.T. Mayer, H. Hoyt, J. Xie, G. McMahon, G. Bischoping, D. Wang, Angew. Chem. Int. Ed. 52 (2013) 12692–12695.
[73] S.C. Warren, K. Voïtchovsky, H. Dotan, C.M. Leroy, M. Cornuz, F. Stellacci, C. Hébert, A. Rothschild, M. Grätzel, Nat. Mater. 12 (2013) 842–849.